Arbitrary pretilt and azimuth angles generation by stacked photoalignment layers

Chung-Yung Lee (SID Member)
Yuet-Wing Li (SID Member)
Man-Chun Tseng (SID Student Member)
Vladimir G. Chigrinov (SID Fellow)
Hoi-Sing Kwok (SID Fellow)

Abstract — We report a method of fabricating a nano-sized stack alignment layer. The stacked alignment layer consists of nano-domains of vertical and planar alignment materials. Experiments reveal that photoalignment thin film can undergo dewetting and form discrete nano-sized domains. Such self-organized structure creates a discontinuous layer stacked on top of a continuous layer and hence produces an inhomogeneous alignment surface. With two or more different principle alignment directions, this new alignment layer is capable of producing multiple pretilt and azimuth angle domains on a single substrate.

Liquid crystal (LC) alignment layer, which controls the LC molecule orientations on the panel surfaces, is one of the most important element to LC display. At present, numerous methods had been proposed for generating pretilt angles in the range of 30°–60°.[1–6] However, there were only a few attempts to produce both variable pretilt and azimuth angles.[4–6] Jong *et al.*[4] had proposed to control the pretilt angles via ion beam irradiation of silicon carbide (SiC) layers of various compositions. The azimuth angle could be controlled by in-plane projection of the particle beam; but the produced pretilt angle only had a limited range of 67° to 90°. Yaroshchuk *et al.*[5] had suggested using plasma beam irradiation to a fluorinated polyimide. Although the produced pretilt angle could be varied from 0° to 90°, the processing window for intermediate values, 30°–60°, was narrow. The transition was nonlinear and like a step function. The azimuth angle had also showed an abrupt change from parallel to perpendicular with respect to the plane of incidence of the plasma beam. In addition, the oblique irradiation might not be favorable to large-area substrate. The spatial reliability remained to be an issue. Ho *et al.*[6] had attempted to generate variable pretilt angles by photoaligning a mixed polyimide. The nano-domains were formed by phase segregation during the drying of mixed fluids.[7] The processing was rather simple, but the repeatability was unsatisfactory because of the uncertainty of the precipitation rate. Hence, in this paper, we would like to propose a stacked nanostructured surface that can fulfill this technology gap. The stacked nanostructured surface is preferable for large-area substrate and is highly reliable. The produced pretilt and azimuth angles can be varied from nearly 0° to 90°. In addition, the processing window is large as the angles are linearly proportional to the nano-domain area ratios. Moreover, we introduce thin film dewetting mechanism for self-generating the nano-domains without resorting to micro-fabrication techniques. The nano-domains of one alignment material are formed on top of another continuous alignment material. Hence, it has a stacked structure with only one additional coating step, which is compatible with existing manufacturing technique. The modeling of this stacked alignment structure had been built. The effects of size and thickness of the nano-domains have been qualitatively studied. The thin-film dewetting phenomenon had also been reviewed. Simulation of the dewetting pattern using LC alignment material had been performed. Experiments of stacked alignment layers, which are composed of a planar-aligned (PA) linear photopolymerizable polymer (LPP) and a vertical-aligned (VA) polyimide, had been performed to check with the modeling. The experimental results had shown a good match with the simulation results. The alignments produced are good quality, robust, reproducible, reliable, and favorable for mass manufacturing.

Wan *et al.*[8] had given detailed study of the homogenized pretilt angle induced by inhomogeneous alignment surface. The homogenized pretilt angle can be modeled by minimizing the total energy of LC bulk and surface energy:

$$F_{\text{total}}\left(\vec{n}\right) = \int_V F\left(\vec{n}\right)dV + \frac{1}{2}\int_S W(x,y)\sin^2\left(\theta - \theta_0(x,y)\right)dS$$

(1)

where $W(x,y)$ and $\theta_0(x,y)$ are the surface energy and the principle pretilt angle at position (x,y) of the simulated cell.[9] $F(\vec{n})$ is the Frank elastic energy density where $\vec{n} \equiv (x,y,z)$ is the unit director of the LC molecule. Considering that all Frank elastic constants K_{ii} are equal and the LC cell consisted of two domains with area ratio p and $1-p$

where $0 \leq p \leq 1$. The period of the surface pattern is denoted by λ. In addition, the pretilt angles of the two domains are θ_1 and θ_2. The extrapolation length is defined by $l_e = \frac{K}{W}$ where W is the polar anchoring strength and K is the Frank elastic constant.[10] For strong polar anchoring alignment layer, e.g., $W \sim 1 \times 10^{-3}$ J/m^2, the extrapolation length is about 10 nm, that is, $l_e \sim 10$ nm. For the case where bulk energy is much larger than surface energy and without twist deformation, that is, $\frac{\lambda p}{l_e} \gg 1$, the analytical solution for homogenized pretilt angle can be obtained by

$$\theta_H = p\theta_1 + (1-p)\theta_2 \qquad (2)$$

The resulting homogenized pretilt angle solely equals to the weighted average of the pretilt angles in the two domains by their area ratio. On the contrary, if the surface energy is much larger than the bulk energy, that is, $\frac{\lambda p}{l_e} \ll 1$, the homogenized pretilt has nonlinear relationship with the domain area ratio p and the anchoring energies of the two domains W_1 and W_2:

$$\theta_H = \theta_1 + \frac{1}{2}\tan^{-1}\left(\frac{(1-p)W_2 \, \sin\, 2(\theta_1 - \theta_2)}{(p-1)W_2 \, \cos\, 2(\theta_1 - \theta_2) - pW_1}\right) \qquad (3)$$

From the aforementioned two extreme cases, it can be observed that the processing window is maximized if and only if the bulk energy dominates the surface energy. Furthermore, in order to make such scenario happen, the dimension of the domain L cannot be too small and must be larger than the extrapolation length, that is, $L = \lambda p \gg l_e \approx 10$ nm. Therefore, to fulfill the bulk effect requirement, the minimum domain size should be at least 10 times larger than the extrapolation length, that is, $L > 100$ nm. However, the domain size cannot be too large in order to avoid the cell gap dependence effect of display applications. Otherwise, the two domains will act like two separate pixels having different optical properties. The minimum cell gap of typical LCD devices is around 3 μm. The domain size should be at least one order less than the cell gap, that is, $L < 300$ nm. The side effect of the pattern on the LC bulk can be ignored in this dimension. Hence, by combining these two constraints, it gives the suitable domain size for inhomogeneous alignment layer, $L \sim 100–300$ nm.

The stacked alignment surface is composed of two layers of different alignment materials. The bottom alignment layer is fixed as a continuous layer, while the top alignment layer is varied with different profiles. We first consider the top alignment layer is also a continuous layer, which covers the bottom alignment layer completely, that is, continuous–continuous. The surface energy of this stacked alignment structure can be modeled by

$$F_S = W_{pt}\sin^2(\theta_H - \alpha_t) + W_{at}\cos^2(\theta_H - \alpha_t)\sin^2(\phi_H - \beta_t)$$

$$+ D^{-\eta}\left[W_{pb}\sin^2(\theta_H - \alpha_b) + W_{ab}\cos^2(\theta_H - \alpha_b)\sin^2(\phi_H - \beta_b)\right] \qquad (4)$$

where W_{pt}, W_{at}, W_{pb}, and W_{ab} account for the polar and azimuthal anchoring strengths of the top and bottom alignment layers, respectively. α_t, β_t, α_b, and β_b define the alignment axes of the top and bottom alignment layers. θ_H and ϕ_H are the homogenized pretilt and azimuth angles imposed by the stacked alignment layers. $D^{-\eta}$ is the exponential decay factor as well as the screening factor. Alexe-Ionescu et al.[11] had suggested that the screening effect can be approximated by the anisotropic "van der Waals-like interaction" form: $D^{-\eta} = h^{-3}$, where h is the thickness of the top alignment layer. Figure 1 plots the homogenized pretilt angle, θ_H, versus different thicknesses of the top alignment layer with different polar anchoring strength ratios. As seen from the figure, the pretilt angle changes notably from α_b to α_t, that is, $\alpha_b \rightarrow \alpha_t$, as the thickness increases from 2 to 5 nm. We further define "fan angle" to be the absolute difference of the azimuth angles between the two layers, that is, $\Delta\beta = |\beta_t - \beta_b|$. The effect of the fan angle is also plotted in Fig. 2. From the calculation, it can be deduced that if the thickness of top alignment layer is larger than 5 nm, the effect of the bottom alignment layer is completely screened out. This critical thickness matched with previous experimental results of Gwag et al.[12]. The abrupt change of the pretilt angles by continuous–continuous stacked structure might be useful for some sensor applications. However, it is not good for LC pretilt angle generation as the processing window is very much limited. Now, let us consider another scenario where the top alignment layer is discontinuous, that is, continuous–discontinuous. For simplicity, we assumed the domain size falls in the suitable range, which has deduced earlier $L \sim 100–300$ nm. Without loss of generality, we further simplified the thickness profile of the top alignment layer $H(x)$ as a step function:
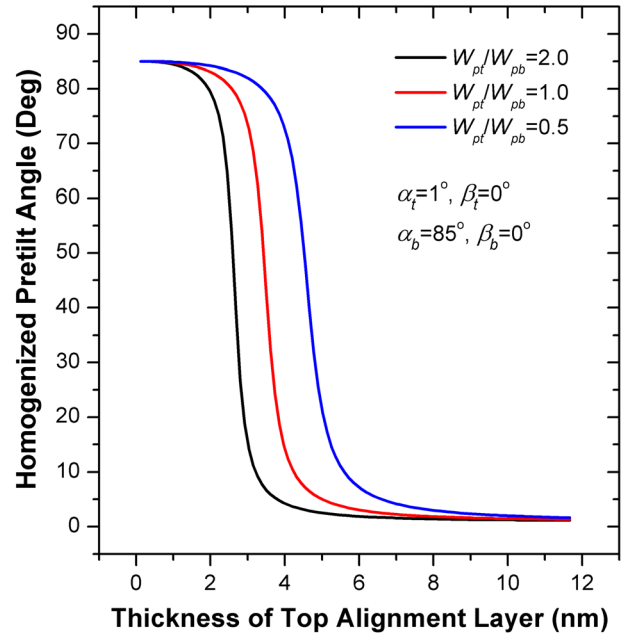

FIGURE 1 — Simulated homogenized pretilt angle of continuous–continuous stacked alignment surface versus different thicknesses of the top alignment layer with different polar anchoring strength ratios.
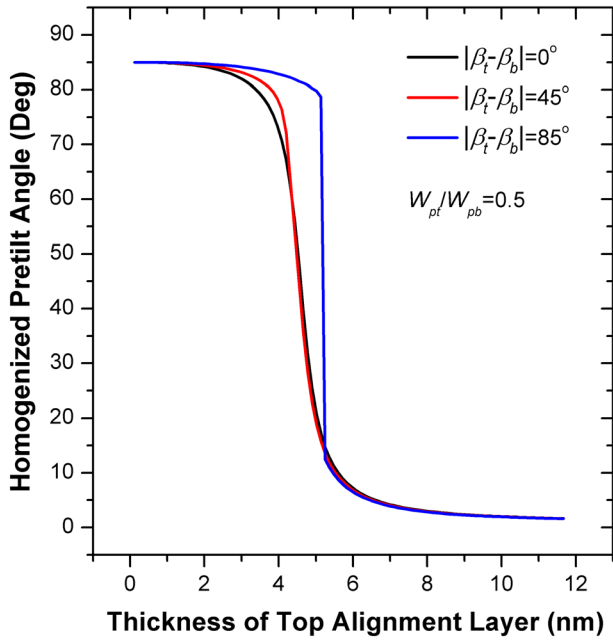
FIGURE 2 — Simulated homogenized pretilt angle of continuous–continuous stacked alignment surface versus different thicknesses of the top alignment layer with different fan angles. The polar anchoring strength ratio was fixed at 0.5.

FIGURE 3 — Simulated homogenized pretilt angle of continuous–discontinuous stacked alignment surface versus different thicknesses of the top alignment layer with different area ratios.

$$H(x) = \begin{cases} h_{\min} & \dfrac{x}{\lambda} > p \\ h_{\max} & \dfrac{x}{\lambda} \le p \end{cases} \qquad (5)$$

where λ is the period of the domain and $x \in [0, \lambda]$. p is the area ratio of the top alignment layer where $0 \le p \le 1$. The simulation parameters were as follows: $h_{\max} \in [0, 12 \text{ nm}]$, $h_{\min} = 0$ nm, $W_{pt} = W_{pb} = 1 \times 10^{-3}$ J/m^2, $W_{at} = W_{ab} = 0.5 \times 10^{-4}$ J/m^2, $(\alpha_t, \beta_t) = (1°, 0°)$, and $(\alpha_b, \beta_b) = (85°, 0°)$. The Frank elastic constants of the LC were as follows: $K_{11} = 14$ pN, $K_{22} = 7$ pN, and $K_{33} = 19$ pN. The simulation result of the homogenized pretilt angle, θ_H, versus different thicknesses of the top alignment layer with different area ratios is plotted in Fig. 3. Likewise, when the thickness is larger than 5 nm, the bottom alignment layer is completely shielded by the top alignment layer. Hence, the homogenized pretilt angle is governed by Eq. (2), which is linearly proportional to the area ratio, p. These results are consistent with the previous continuous–continuous case. The effect of the fan angle is plotted in Fig. 4 where the area ratio, p, is fixed at 0.5. The homogenized pretilt angle increases slightly as the fan angle increases. Such result can be explained in terms of LC bulk elastic energy. As the fan angle introduces a twist deformation, LC molecule will vary its pretilt angle in order to minimize the additional twist elastic energy. For LC material, which favors splay deformation more than the bend deformation, that is, $K_{33} > K_{11}$, the pretilt angle will increase. In contrast, the pretilt angle will drop if the LC material has $K_{11} > K_{33}$. Hence, the continuous–discontinuous stacked alignment structure has a much larger
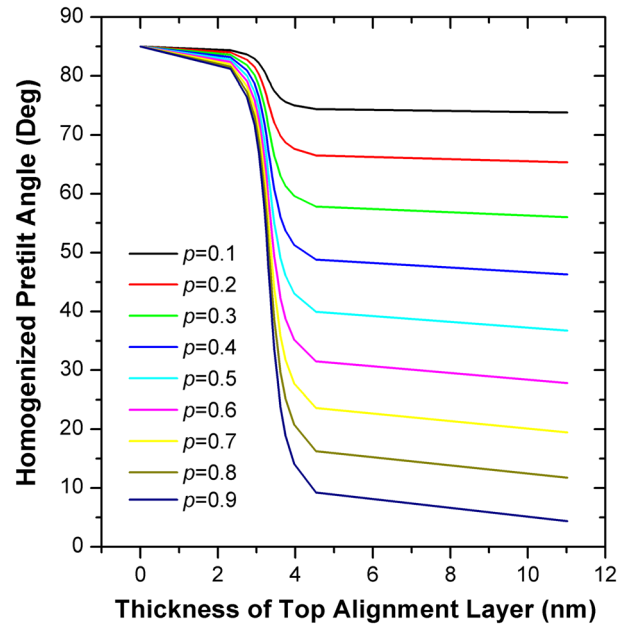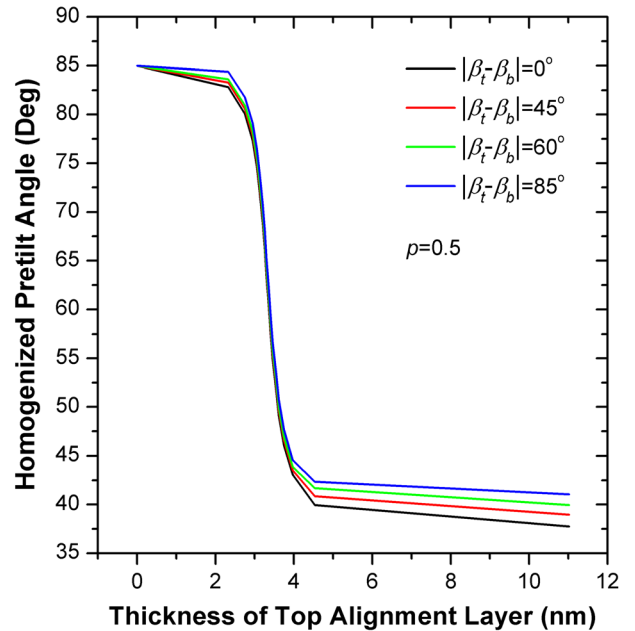

FIGURE 4 — Simulated homogenized pretilt angle of continuous–discontinuous stacked alignment surface versus different thicknesses of the top alignment layer with different fan angles. The area ratio was fixed at 0.5.

processing window for LC pretilt angle generation. Figures 5 and 6 plot the homogenized pretilt and azimuth angles versus different area ratios. The thickness of the top alignment layer is fixed at 5 nm, which is thick enough to avoid the nonlinear effect. It can be found that the homogenized pretilt and azimuth angles, (θ_H, ϕ_H), gradually change from (θ_b, ϕ_b) to (θ_t, ϕ_t). Moreover, as fan angle increases, the
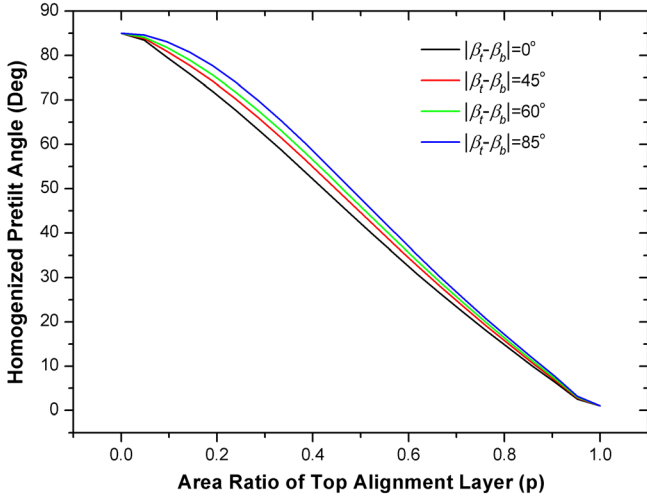
FIGURE 5 — Simulated homogenized pretilt angle of continuous–discontinuous stacked alignment surface versus different area ratios of the top alignment layer with different fan angles.
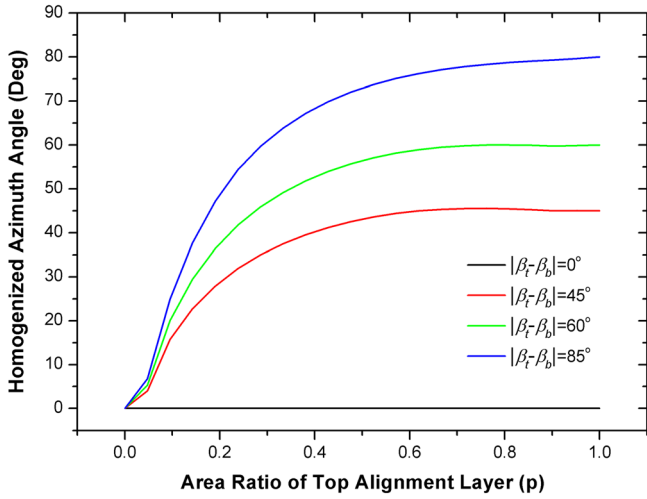

FIGURE 6 — Simulated homogenized azimuth angle of continuous–discontinuous stacked alignment surface versus different area ratios of the top alignment layer with different fan angles.

corresponding pretilt angle also rises owing to the twist effect. These simulation results of stacked alignment surfaces were consistent with previous experimental results of Zhang et al.[13] where they called double-layer alignment film. Hence, our proposed model for stacked alignment surface is accurate and comprehensive.

In this work, we focus on the continuous–discontinuous stacked alignment structure as we want to control the pretilt and azimuth angles for the LC devices. The structure of the proposed stacked alignment layers is drawn in Fig. 7. The stacked alignment surface is composed of two layers of different alignment materials. The bottom alignment layer is a continuous layer, while the upper one is a discontinuous layer. As derived from the preceding text, such structure has the maximum processing window for generating LC pretilt angle. The most important feature of the experiment
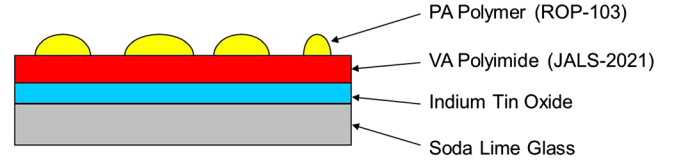

FIGURE 7 — Schematic structure of the proposed stacked alignment surface. PA, planar aligned; VA, vertical aligned.

is to obtain both continuous and discontinuous alignment layers at the right position and order. Our proposed method relies on dewetting of thin liquid film. The self-organized dewetting formation is generally regarded as one of the most promising bottom-up approaches for fabricating nano-domains structure without the need of using any photomask.

Consider a thin liquid film on a non-wettable substrate. The liquid film is not stable and will bead up.[14–17] The viscous flow is considered as the dominant mechanism. The dynamics is driven by pressure gradients within the film, which are primarily dominated by the surface energy of the thin liquid film and the effective interface potential to the substrate. When a thin liquid film beads off a solid substrate, it is eventually transformed into an ensemble of individual liquid droplets, the arrangement of which may vary strongly according to the dewetting process. The free energy of a thin liquid film on a substrate can be written as[18]

$$H(h) = \int \left(\frac{\gamma}{2} (\nabla h)^2 + \varphi(h) \right) d\vec{x} \qquad (6)$$

where $\vec{x}$ denotes a spatial point within the two-dimensional substrate, γ is the surface tension, h is the thickness of the thin film, and $\phi(h)$ is the effective interface potential. This expression comprises a long-wavelength approximation for the capillary energy with surface tension and effective interface potential that covers intermolecular forces beyond capillarity. Seemann et al.[19,20] had suggested that the effective interface potential of this system can be expressed by

$$\phi(h) = \frac{B}{h^8} - \frac{A}{12\pi h^2} \qquad (7)$$

where B denotes the strength of the short-range part of the potential and A is the Hamaker constant. The effective interface potential is also known as the excess free energy per unit area. It is composed of antagonistic, that is, attractive and repulsive, long-range and short-range interactions. The first term, $\frac{B}{h^8}$, includes the short-range interactions of strength B, whereas the second term, $\frac{A}{12\pi h^2}$, characterizes the long-range interactions by the van der Waals potential. The spinodal dewetting can only take place when the second derivative of $\phi(h)$ with respect to the film thickness is

negative, that is, $\phi''(h_o) < 0$, where h_0 is the initial homogeneous film thickness. The expression can be further derived to obtain the critical thickness, h_c:[21,22]

$$h_c = 2\sqrt{\frac{\gamma}{\rho g}}\sin\left(\frac{\theta_e}{2}\right) \qquad (8)$$

where γ is the surface tension, ρ is the liquid density, g is the gravitational constant, and θ_e is the equilibrium contact angle. A film with $h_0 \geq h_c$ is stable. But if the film is forced to adopt a thickness smaller than h_c, spinodal dewetting will occur until its thickness becomes equal or larger than h_c. Typically, $h_c \approx 10$ nm for nano-scopic thin film. Such phenomenon results in a discontinuous thin film layer. According to the literature,[23,24] the size of these thin film droplets is a function of the film thickness and the interface potential of the coated surface. That is, once spinodal dewetting occurs, there is a certain wavelength, λ_s, the amplitude of which grows fastest, leading to a characteristic emerging dewetting pattern of the liquid film.

$$\lambda_s(h) = \sqrt{-\frac{8\sigma\pi^2}{\phi''(h)}} \qquad (9)$$

In other words, for our application, the patterned domain island of the alignment layer can be extremely uniform by carefully controlling the experimental environment. Such feature allows mass manufacturing of large-scale display panel. Figure 8 shows the simulated dewetting pattern of different initial film thicknesses, (a) $h_0 = 3$ nm, (b) $h_0 = 4$ nm, and (c) $h_0 = 5$ nm, where $\gamma = 60$ mN/m, $\eta = 30$ mPas, $A = 5.3 \times 10^{-19}$ J, and $B = 6 \times 10^{-75}$ Jm^6. For the details of the dewetting modeling, please refer to our another published article.[25]

In order to verify the theory, several experiments had been carried out. The details of experiment steps were as follows: Firstly, several well-cleaned indium tin oxide (ITO) glass substrates were prepared. Figure 9 shows the atomic
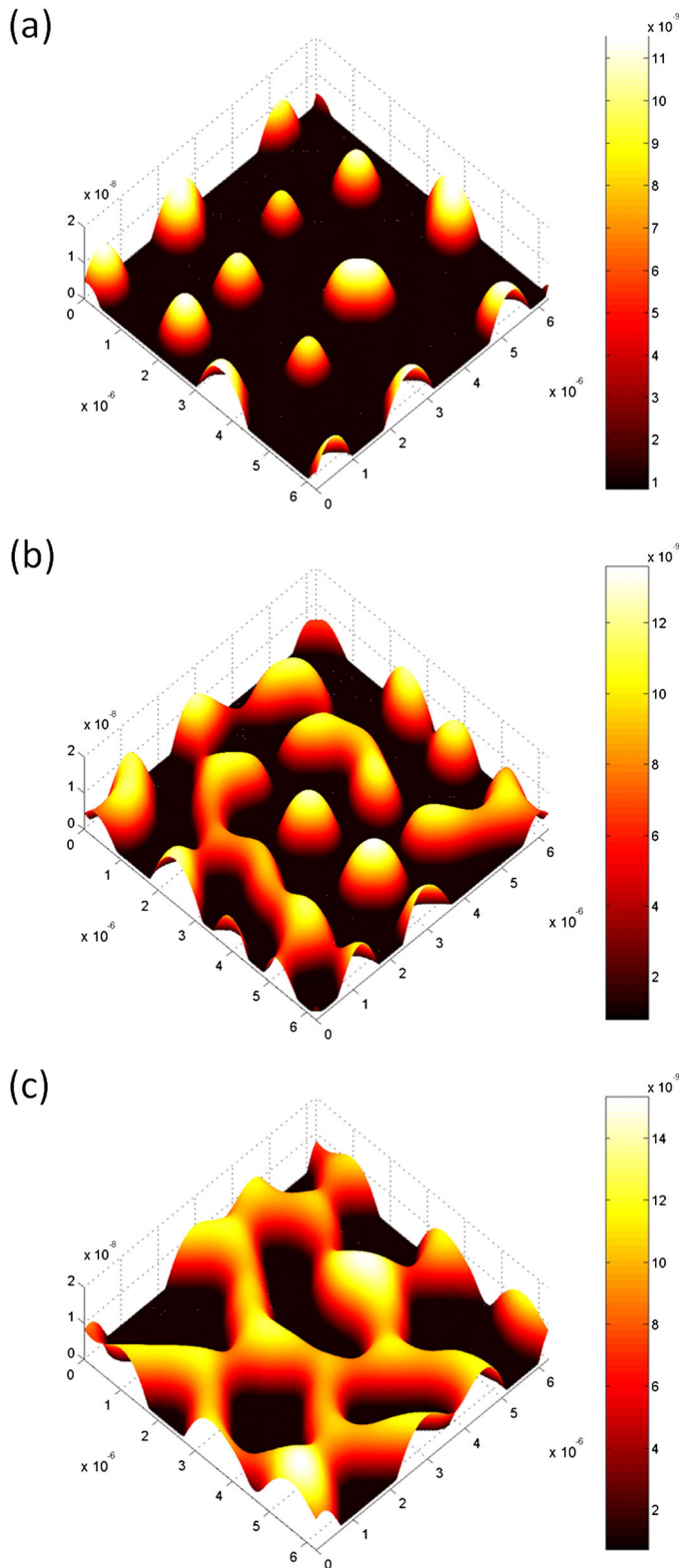

(a)

(b)

(c)

FIGURE 8 — Simulated dewetting patterns of different initial film thicknesses: (a) 3, (b) 4, and (c) 5 nm. The surface tension was 60 mN/m.
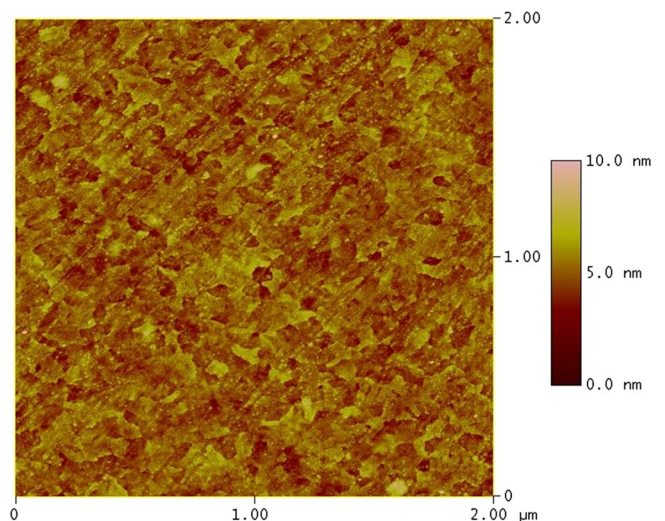

FIGURE 9 — Atomic force microscopic picture of an indium tin oxide glass substrate.
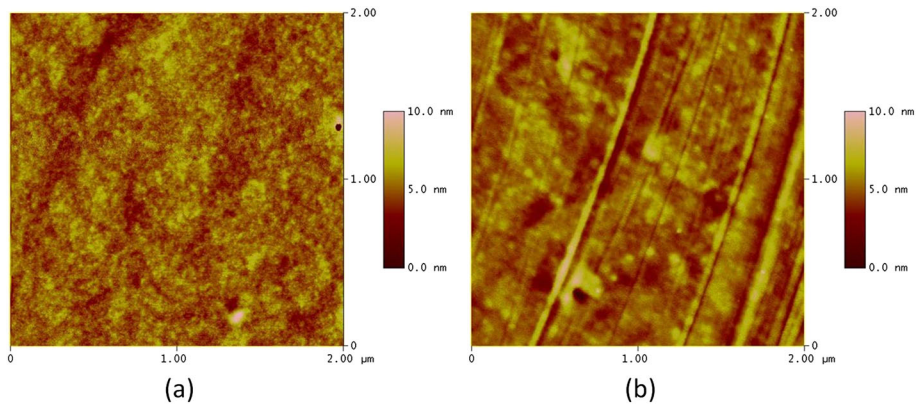
FIGURE 10 — Atomic force microscopic picture of the continuous vertical-aligned polyimide alignment layer, JALS-2021, (a) before and (b) after mechanical rubbing.
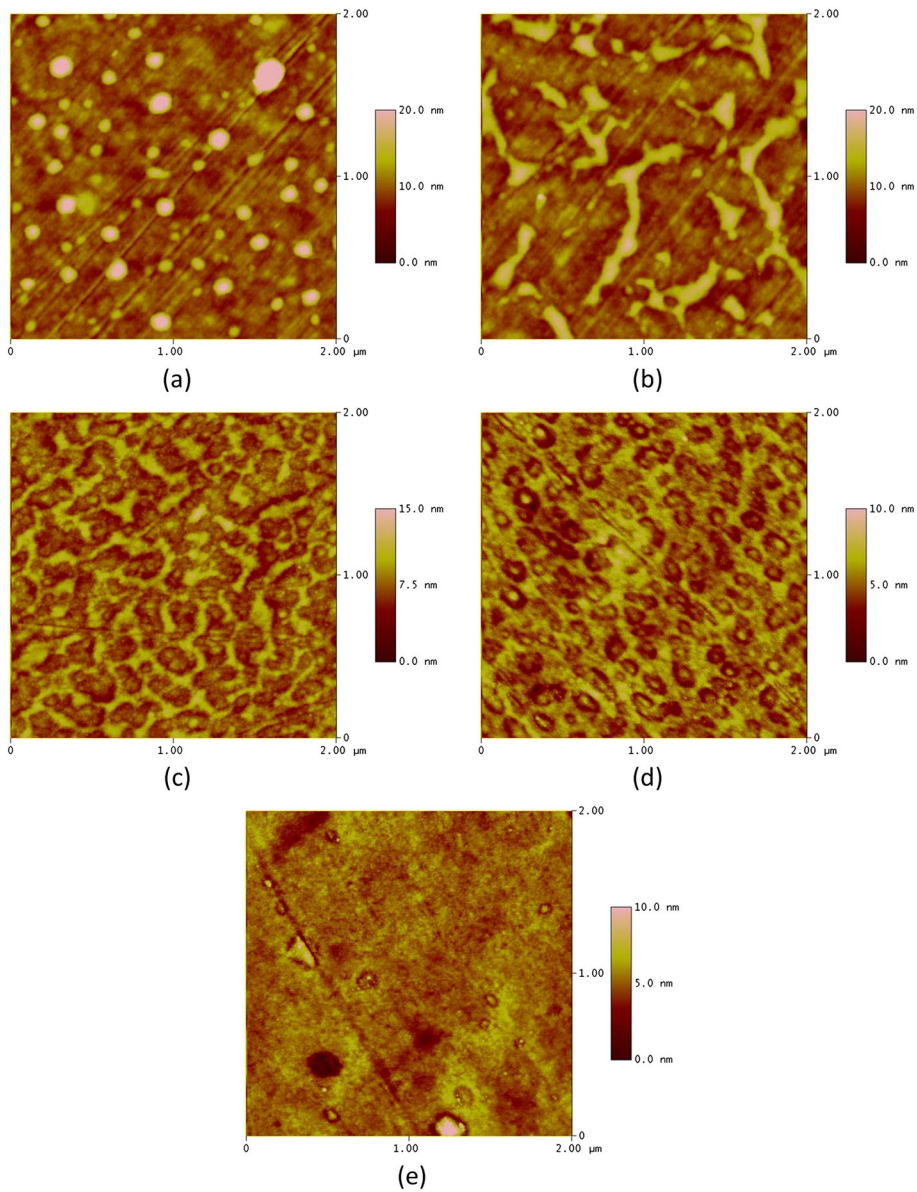

FIGURE 11 — Atomic force microscopic picture of the discontinuous planar-aligned linear photopolymerizable polymer (LPP) alignment layer, ROP-103, with different concentrations: (a) 0.02, (b) 0.04, (c) 0.06, (d) 0.08, and (e) 0.1 wt%. The LPP alignment layer is stacked on top of the polyimide layer.

force microscopic (AFM) picture of the ITO crystalline pattern of the glass substrate. Secondly, a VA polyimide JALS-2021 from JSR Corporation (Tokyo, Japan) was spin-coated on the ITO glass substrates at 3000 rpm for 180 s. Then the glass substrates were baked inside the oven at 230°C for 90 min. It was expected that no dewetting would occur during the baking as the film thickness of the polyimide was thick, $h_0 > 100$ nm. Figure 10(a) proves this prediction; the ITO crystalline patterns were completely covered by the continuous polyimide layer. Before coating the upper layer, the substrates were rubbed by a rubbing cloth to obtain the first principle pretilt and azimuth angles (θ_1, ϕ_1). Figure 10(b) shows the AFM picture of the VA polyimide layer after rubbing. Rubbing lines scratched by the velvet cloth can be clearly observed in the picture. After that, the rubbed substrates were further coated with different weighted concentrations of a LPP, ROP-103, provided by Rolic Technology Ltd (Allschwil, Switzerland). The LPP provided PA to LC molecules with a small pretilt angle. The concentrations of the ROP-103 could be adjusted by using the solvent cyclohexanone and was varied from 0.02 to 0.1 wt%. As a result, different concentrations of ROP-103 would induce different film thicknesses. Similar to the previous coating steps, the ROP-103 was also spin-coated on the substrate with spinning speed of 3000 rpm for 60 s. Afterward, the substrates underwent soft-baking at 130°C for 5 min on a hot plate. At the end, the substrates were exposed by linear polarized ultraviolet (LPUV) light source with wavelength 280–340 nm at normal incident angles. The dosage was about 200 mJ/cm^2. The azimuthal orientation direction of the LPP was defined parallel to the plane of LPUV polarization, so that the second principle pretilt and azimuth angles (θ_2, ϕ_2) were obtained. Because low-viscosity solvent cyclohexanone was applied, the thickness of the ROP-103 layer was expected to be very thin and dewetting should occur. Figure 11 shows the AFM picture of the stacked alignment layers with (a) 0.02, (b) 0.04, (c) 0.06, and (d) 0.08 wt% concentrations of ROP-103 solution. It can be observed that the upper alignment layers are indeed discontinuous and the period of the domains are quite uniform. As the concentration of ROP-103 increases, the thickness of the alignment layer will also increase. Eventually, the solution cannot undergo dewetting. Figure 11(e) shows a continuous ROP-103 alignment layer with 0.1 wt% concentration.

From the AFM pictures, it can be found that the average domain size, L, is about 100 to 300 nm. Such domain size is suitable for generating pretilt angles of LC display. There are two reasons. First, the domain sizes are much larger than the extrapolation length, $l_e \approx 10$ nm. As a result, $\frac{\lambda_p}{l_e} \gg 1$, the bulk energy is much larger than the surface energy. The homogenized pretilt angle should be linearly proportional to the domain ratio, p. The second reason is the domain sizes are one order smaller than the typical cell gap of the LC display, which is about 3 to 5 μm. Hence, the cell gap dependence
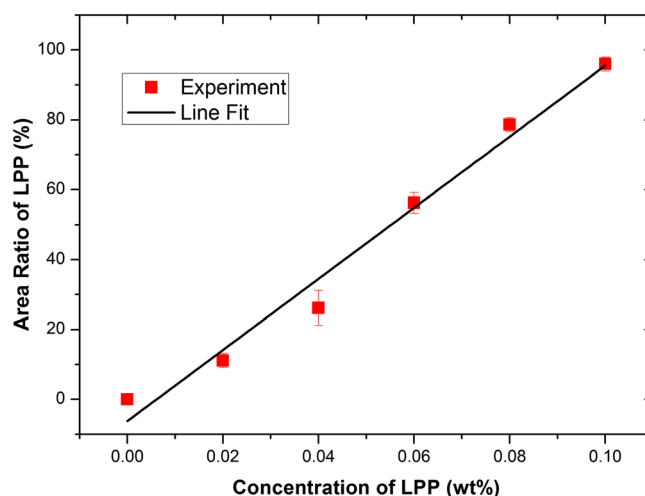

FIGURE 12 — The area ratios of the top linear photopolymerizable polymer (LPP) layer with regard to different LPP concentrations.
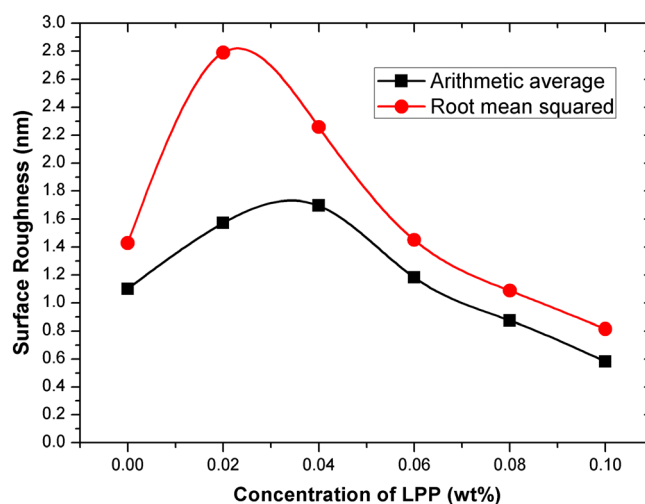

FIGURE 13 — The arithmetic average and root mean squared surface roughness of different concentration linear photopolymerizable polymer (LPP) samples.
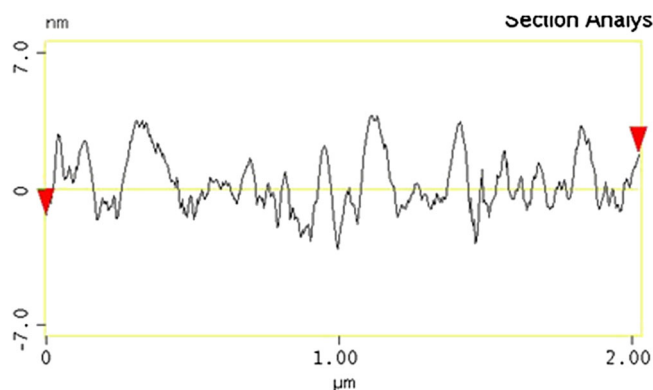

FIGURE 14 — Atomic force microscopic section analysis of a 0.06 wt% linear photopolymerizable polymer concentration sample.
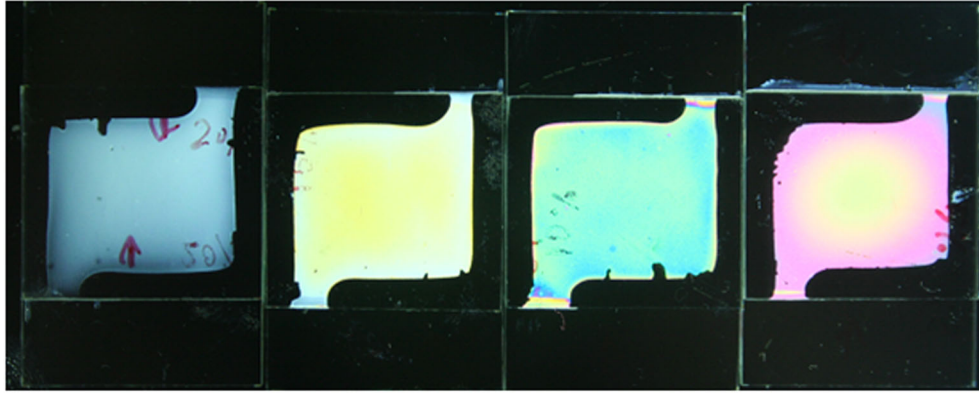
FIGURE 15 — Photo of the 0.02, 0.04, 0.06, and 0.08 wt% (from left to right) samples placed under a pair of crossed polarizers.

effect can be avoided. By applying simple image processing to the AFM pictures, we can obtain the area ratio of the top PA LPP layer with regard to different LPP concentrations,

$$p = \frac{\text{Area}_{\text{PA}}}{\text{Area}_{\text{PA}} + \text{Area}_{\text{VA}}} \qquad (10)$$

The Area_{PA} corresponded to the top layer PA LPP (ROP-103) material, while the Area_{VA} corresponded to the bottom uncovered layer VA polyimide (JALS-2021) material. The result is plotted in Fig. 12. The area ratio is almost linear to the weighted concentration; hence, the processing window should be large. Both the arithmetic average and root mean squared surface roughness of different-concentration LPP samples are shown in Fig. 13. We further analyzed the thickness of the formed nano-sized island domains. Figure 14 shows the section analysis of a 0.06 wt% sample. The thickness of the islands is >5 nm, which is thick enough to completely shield the alignment effect of its bottom layer and avoid the nonlinear thin layer stacked effect.
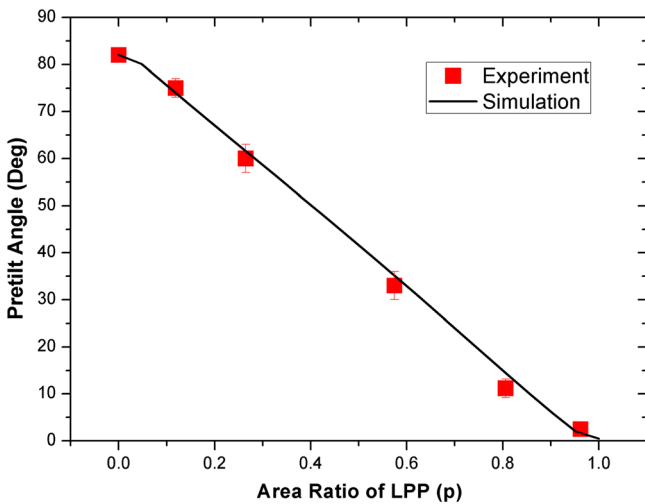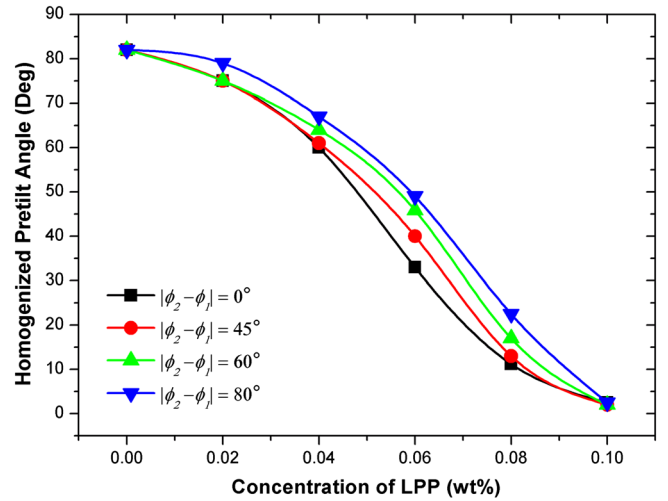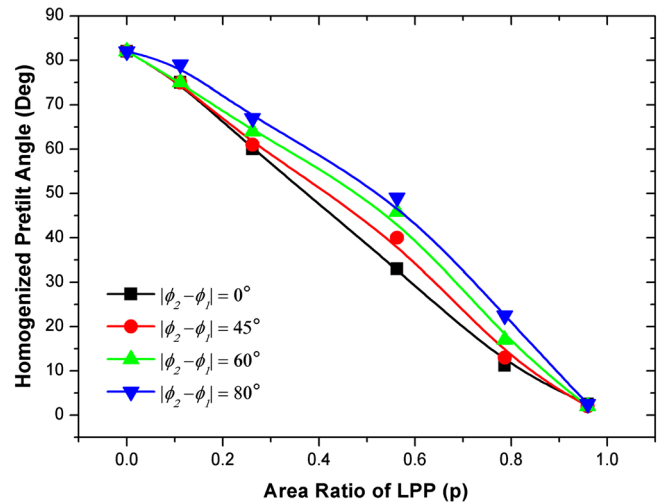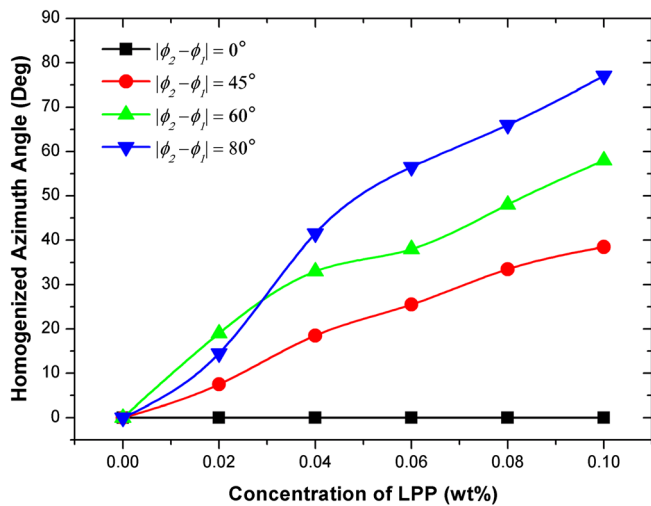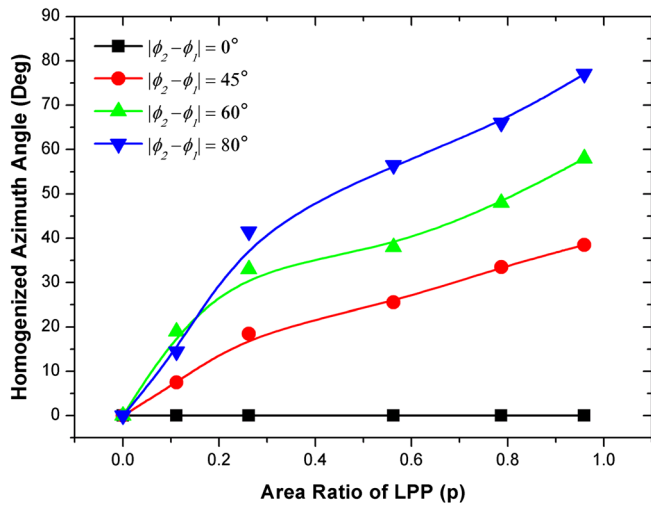

(a)

(b)

FIGURE 17 — Measured homogenized pretilt angles θ_H versus different (a) concentrations wt% and (b) area ratios p of linear photopolymerizable polymer (LPP) for $|\varphi_2 - \varphi_1| > 0$.

FIGURE 16 — Measured homogenized pretilt angles θ_H versus different area ratios p of linear photopolymerizable polymer (LPP) for $|\varphi_2 - \varphi_1| = 0$.

By using the stacked alignment layers, two principle alignment directions $(\theta_1 = 87, \phi_1)$ and $(\theta_2 = 0.5, \phi_2)$ can be generated by JALS-2021 and ROP-103, respectively. Several LC cell samples were fabricated to measure their homogenized pretilt and azimuth angles, (θ_H, ϕ_H). The cells were assembled in antiparallel structure with stacked alignment layers on both substrates. The cell gap was $5\,\mu m$ and was filled with LC MLC-6080 $(\Delta n = 0.2024)$ from Merck Corporation (Darmstadt, Germany). Figure 15 shows the photo of the 0.02, 0.04, 0.06, and 0.08 wt% samples placed under a pair of crossed polarizers. As shown in the photo, the quality of LC alignment in the cells produced by the proposed method is good. Their azimuth angles were first determined under a polarized light microscope. Then the pretilt angles were measured by using the crystal rotation method.[26] For the case $|\phi_2 - \phi_1| = 0$, Fig. 16 shows a linear relationship between the area ratio and the pretilt angle. Such result agrees with the theory and proves that the bulk effect dominates the pretilt angle generation. Hence, the processing window is maximized. For the case $|\phi_2 - \phi_1| > 0$, a new parameter is induced: homogenized azimuth angle ϕ_H. Figures 17 and 18 show the effect of the case $|\phi_2 - \phi_1| > 0$ on the homogenized pretilt and azimuth angles. From Fig. 17, it can be found that as the $|\phi_2 - \phi_1|$ becomes larger, the pretilt angle with the same area ratio will always become slightly higher. The reason is properly due to the twist elastic energy induced by $|\phi_2 - \phi_1|$ such that the homogenized pretilt angle has to increase to minimize the elastic energy caused by the twist effect. Furthermore, as the concentration of the LPP increases, (θ_H, ϕ_H) will eventually equal to (θ_2, ϕ_2). This result is very important as it proved that the top alignment layer is not only continuous but also thick enough to completely shield the bottom alignment layer. Hence, we can consider the top and bottom alignment layers into two independent domains. The corresponding polar anchoring energy of different homogenized pretilt angle was measured by using high voltage method[27] as shown in Fig. 19. The average value is about $1.2\,mJ/m^2$. Such value is comparable with conventional polyimide. The bottom alignment layer is simply conventional polyimide, having the polar anchoring energy strength about $0.8\,mJ/m^2$. And the polar anchoring energy strength of the top layer photoalignment polymer, ROP-103, was measured to be $1\,mJ/m^2$. The trend of the polar anchoring is increasing with the homogenized pretilt angles. Such observations are consistence with measurement results of Murauski et al.[28]

The reproducibility of the stacked alignment layers had been checked. Specimens of different concentrations of LPP were tested. For each concentration, 10 sample sets had been fabricated. The homogenized pretilt and azimuth angles were then measured. The results are shown in Fig. 20(a) and 20(b).

(a)

(b)

FIGURE 18 — Measured homogenized azimuth angles φ_H versus different (a) concentrations wt% and (b) area ratios p of linear photopolymerizable polymer (LPP) for $|\varphi_2 - \varphi_1| > 0$.
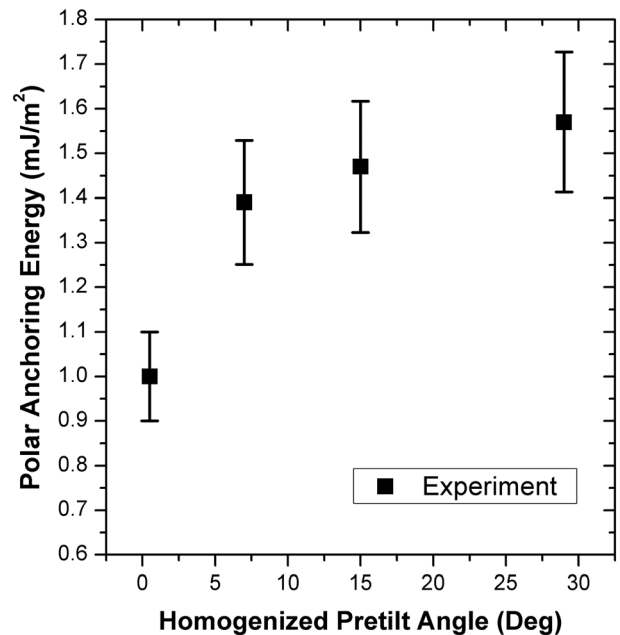

FIGURE 19 — Measured polar anchoring energy for different homogenized pretilt angles.
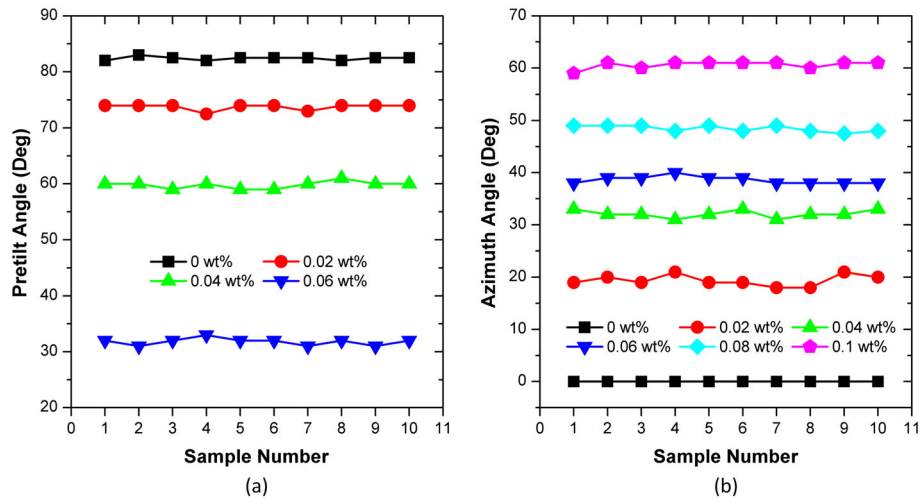
FIGURE 20 — Reproducibility test of homogenized (a) pretilt and (b) azimuth angles with 10 fabricated sample sets for the stacked alignment layers.

The deviations of both angles for all 10 samples were less than 2°, which is acceptable for most of the applications. The reasons for the highly repeatable results are twofold. Firstly, the nonlinear effect induced by the anchoring energy is prevented because of the desirable domain size. Secondly, all the materials used in the experiment are commercially available. They are robust and of high quality. The effect of LPP polymerization time to the stacked alignment layers was also investigated. The power of the LPUV source was about 5 mW. Several samples with the same concentration of LPP, but using different polymerization time, had been fabricated. The measured pretilt angles are shown in Fig. 21. The pretilt angle remained unchanged when the polymerization time was longer than

400 s. The reason is that once the irradiation exceeds the required dosage, the LPP material becomes fully polymerized. Hence, the domain size and the azimuthal alignment direction cannot be changed anymore. The stacked alignment layers were found stable against temperature cycling up to 100 °C. The results are shown in Fig. 22. Four different samples with different pretilt angles were put into a 100 °C oven after they had been end-sealed. Their pretilt angles were checked every 2 h interval after the samples were cooled down. It was found that the pretilt angles remained almost unchanged throughout the experiment. The operating temperature range of the stacked alignment layers had also been checked. Figure 23 shows the pretilt angles measurement of a 0.06 wt% LPP
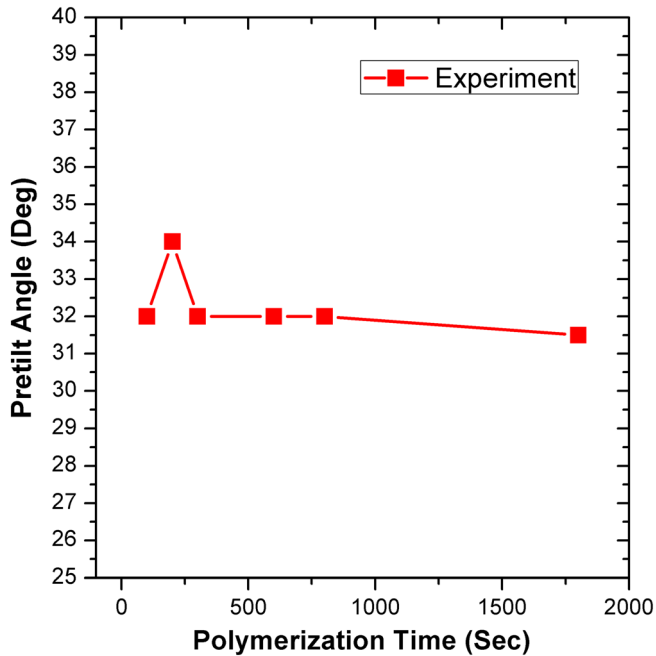

FIGURE 21 — The homogenized pretilt angle dependence on the linear polarized ultraviolet polymerization time for linear photopolymerizable polymer.
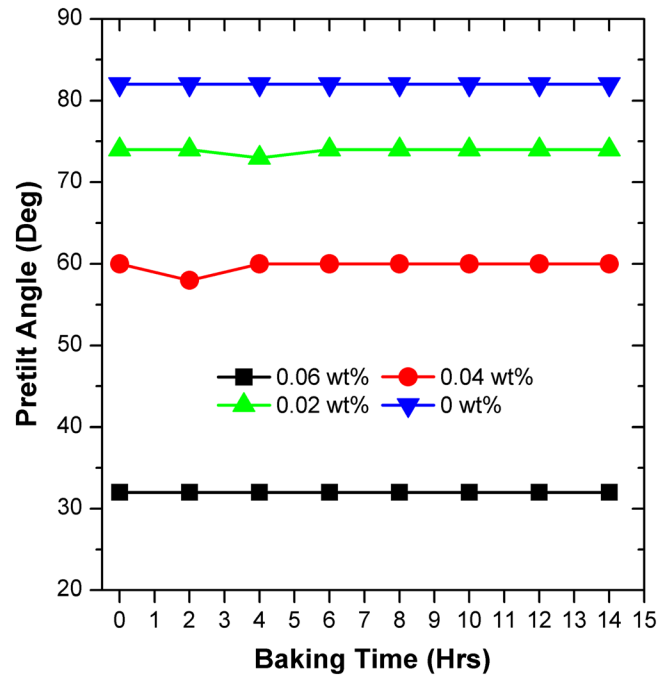

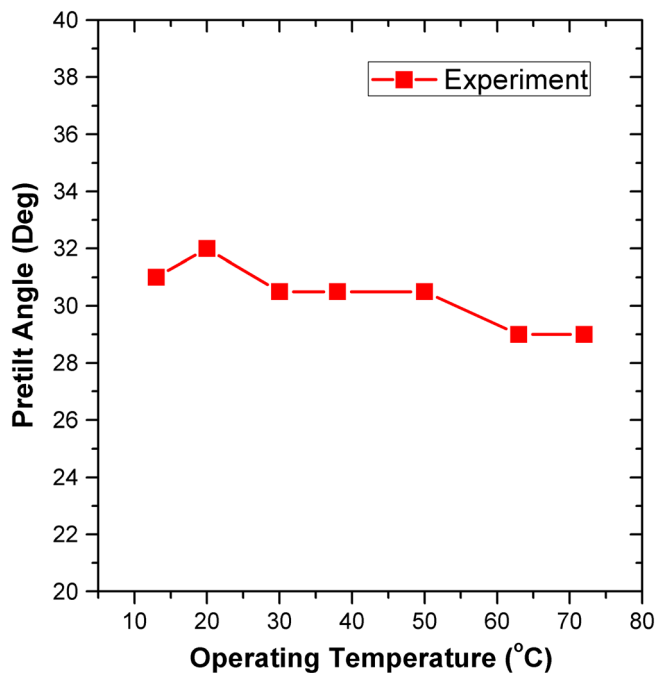**FIGURE 22** — Temperature cycling test for the stacked alignment layers.

FIGURE 23 — The fluctuation of the homogenized pretilt angle of a 0.06 wt% sample operating between temperatures 10 and 80 °C.

sample cell operating between temperatures 10 and 80 °C. The sample was filled with LC MLC-6080, provided by Merck Corporation. The clearing temperature of the LC is 95 °C. The sample was put on a metal heater stage. The stage was allowed to rotate for the pretilt angle measurement. The temperature of the sample was monitored by a digital thermometer. The pretilt angle remained almost constant throughout the test. In fact, this temperature behavior is similar to the ordinary polyimide.[29] Thus, the proposed new alignment layers described here are practical for common LC displays.

In conclusion, we have demonstrated a practical method to generate multiple and arbitrary pretilt and azimuth angles for LC devices. Such effect is particularly useful for LC switchable focal lens,[30] wave-guide devices,[31] fast-response displays,[32] bistable displays,[33] multi-domains displays,[34] and LC dynamic flow control studies.[35] The processing window of such method has been maximized. As the self-organized domains are very uniform, highly reproducible results can be obtained even for large-area manufacturing.

Acknowledgment

References

1 X. Lu et al., Appl. Phys. Lett., **88**, 243508 (2006).
2 F. S. Y. Yeung et al., J. Appl. Phys., **99**, 124506 (2006).
3 C. Y. Lee et al., J. Soc. Inf. Display, **21**, 407 (2014).
4 J. B. Kim et al., Appl. Phys. Lett., **90**, 043515 (2007).
5 O. V. Yaroshchuk et al., Phy. Rev. E, **77**, 031706 (2008).
6 J. Y. L. Ho et al., Appl. Phys. Lett., **90**, 243506 (2007) .
7 H. S. Kwok and F. S. Y. Yeung, J. Soc. Inf. Display, **16**, 911 (2008).
8 J. T. K. Wan et al., Phy. Rev. E, **72**, 021711 (2005).
9 S. Faetti, "Anchoring effects in nematic liquid crystals," in Physics of Liquid Crystalline Materials, I. C. Khoo and F. Simoni, (eds.), (1991), pp. 301–336.
10 P. G. Gennes and J. Prost, The Physics of Liquid Crystals, (1995), pp. 114–113.
11 A. L. Alexe-Ionescu et al., Appl. Phys. Lett., **66**, 1701 (1995).
12 J. S. Gwag et al., J. Appl. Phys., **100**, 093502 (2006).
13 K. Zhang et al., Liquid Crystals, **35**, 1191 (2008).
14 G. Reiter, Phys. Rev. Lett., **68**, 75 (1992).
15 R. Xie et al., Phys. Rev. Lett., **81**, 1251 (1998).
16 C. Vree and S. G. Mayr, Appl. Phys. Lett., **94**, 093110 (2009).
17 J. Bischof et al., Phys. Rev. Lett., **77**, 1536 (1996).
18 J. Becker et al., Nat. Mater., **2**, 59 (2003).
19 R. Seemann et al., J. of Phys.: Condensed. Matter, **13**, 4925 (2001).
20 R. Seemann et al., Phys. Rev. Lett. **86**, 5534 (2001).
21 A. Sharma and E. Ruckenstein, J. of Colloid and Interface Science, **133**, 358 (1989).
22 D. Gentili et al., Chem. Soc. Rev., **41**, 4430 (2012).
23 R. Seemann et al., Phys. Rev. Lett. **87**, 196101 (2001).
24 A. Sharma and R. Khanna, Phys. Rev. Lett. **81**, 3463 (1998).
25 C. Y. Lee et al., "Nano-domains formation on photoalignment thin film by self-organized dewetting," J. Soc. Inf. Display (2015). DOI: 10.1002/jsid.282
26 S. Koichiro et al., Jap. J. Appl. Phys. **34**, 4905–4908 (1995).
27 Y. A. Nastishin et al., Appl. Phys. Lett., **75**, 202 (1999).
28 A. Murauski et al., Phy. Rev. E, **71**, 061707 (2005).
29 F. S. Yeung et al., Appl. Phys. Lett., **88**, 051910 (2006).
30 M. C. Tseng et al., J. Appl. Phys., **109**, 083109 (2011).
31 F. Fan et al., Opt. Express, **20**, 23036 (2012).
32 F. S. Yeung et al., Appl. Phys. Lett., **88**, 041108 (2006).
33 Y. W. Li and H. S. Kwok, Appl. Phys. Lett., **95**, 181107 (2009).
34 Y. W. Li et al., SID Sym. Dig. Of Tech. Papers, **39**, 1026 (2008).
35 Y. W. Li et al., Appl. Phys. Lett., **94**, 061111 (2009).

Dr. Chung Yung Lee received his PhD, MPhil, and BEng degrees from Hong Kong University of Science and Technology in 2013, 2009, and 2007, respectively. He is currently a Research Fellow of the State Key Laboratory on Advanced Displays and Optoelectronics Technologies, HKUST. He is also a member of Society of Information Display. He has been researching on liquid crystal display for more than 8 years. He has over 40 international publications, including patents, book chapter, journals, and conference papers. His research topics include liquid crystal alignment surface, fast-response time liquid crystal mode, three-dimensional display, and bistable liquid crystal display.

Dr. Yuet-Wing Li received his PhD degree from Hong Kong University of Science and Technology in 2009. His research topics include fast response time LCD and liquid crystal alignment. He has been employed by Himax Display Inc. (Taiwan) as a Technical Manager after his graduation.

Man Chun Tseng is currently a PhD student of the Hong Kong University of Science and Technology and under the supervision of Prof. Hoi Sing Kwok. He received his BEng and MPhil degrees in 2007 and 2010, respectively.

Professor Vladimir G. Chigrinov obtained his PhD degree in solid state physics (liquid crystals) in 1978 in the Institute of Crystallography, USSR Academy of Sciences. Since 1996, he was working as a leading scientist in the Institute of Crystallography, Russian Academy of Sciences and join HKUST in 1999, as an associate professor. He was a coauthor of a pioneering work in LC photoaligning technology and ferroelectric LC materials, which has about 500 citations in scientific and technical journals. He is an expert in flat panel technology in Russia and became a fellow of SID since 2008. Since 1997, he is the Vice President of Russian Chapter of SID. He is a member of the Editorial Board of 'Liquid Crystals Today' since 1996 and Associate Editor of *Journal of SID* since 2005. He is also a member of the International Advisory Committee for Advanced Display Technology Conferences in Russia, Ukraine, and Belarus since 1999, European SID Program Committee since 2004, and International Advisory Board of International Liquid Crystal Conference since 2006. He is an author of 2 books, 15 reviews and book chapters, 133 journal papers, 286 conference presentations, and 50 patents and patent applications in the field of liquid crystals since 1974.

Professor Hoi Sing Kwok received his BS degree in electrical engineering from Northwestern University in 1973. He then studied at Harvard University, where he received his MS and PhD degrees in applied physics in 1974 and 1978, respectively. From 1978 to 1980, he worked at the Lawrence Berkeley Laboratory. From 1980 to 1992, he was with the Department of Electrical and Computer Engineering, State University of New York at Buffalo, where he was a full professor since 1985. He joined HKUST in 1992. He is currently the Dr William M W Mong Chair Professor of Nanotechnology of the Department of Electronic and Computer Engineering and the Director of the State Key Laboratory on Advanced Displays and Optoelectronics Technologies at HKUST. Professor Kwok is active in professional activities. He Has chaired and was a member of program committees of many international conferences. He was awarded a Presidential Young Investigator Award in 1984 and the New York State and UUP Excellence Award in 1991. He is a fellow of IEEE, OSA, and SID. He is also an elected member of the Asia Pacific Academy of Materials. Professor Kwok has published over 500 journals and conference papers. He has also edited six conference proceedings and holds more than 10 patents. His latest book on Modeling and Optimization of LCD Optical Performance (coauthored with Prof. Chigrinov) has came out in 2015.